Multiple peptide conformations give rise to similar binding affinities: molecular simulations of p53-MDM2

Shubhra Ghosh Dastidar, David P. Lane, Chandra S. Verma

Supporting information

(List and order of the references are independent of the main text)

Method: The initial structure of the wild type MDM2-p53 complex used for this study was obtained from the protein data bank (PDB code 1YCR, resolution 2.6Å).[1] Only residues 17-29 of p53 and 25-109 of MDM2 were used as their densities were well resolved in the crystal structure. The N- and C-termini of p53 and MDM2 were capped by acetyl (ACE) and N-methyl (NME, $-NHCH_3$) groups respectively. The structures of the W23L and P27Sc mutants of p53 were prepared by replacing the side chain of wild type p53 and generating the coordinates of the side chain atoms.

Each system (complexes, uncomplexed MDM2, peptides) was solvated with TIP3P water and charges were neutralized by adding counter ions resulting in ~14000 atoms. The structures were minimized initially with the backbone atoms fixed and finally with all constraints removed. This was followed by molecular dynamics simulations (each simulation was carried out for 18-20ns) at 300K using the CHARMM22 force field.[2] Non-bonded cutoffs were truncated at 12Å although long range electrostatic interactions were calculated using the Particle Mesh Ewald (PME) technique.[3] Periodic boundary condition was applied and the thickness of the water-box ensured that the protein-complex and its image were always separated by at least 18-20Å. SHAKE[4] was applied to freeze the vibration of the bonds involving hydrogen, enabling a 2fs integration time step; data was saved every 2ps. The systems associated with the various simulations (trajectories) are summarized in Table S1. The binding enthalpies were calculated using the MMGBSA methodology, employing the GBSW[5,6] module of CHARMM while the entropies were calculated using vibrational frequencies derived from normal mode computations. In order to ensure that the systems had relaxed sufficiently, calculations were carried out

over the last 10ns segment of each trajectory. For binding enthalpy calculation structures were chosen every 2ps, and for entropy calculations, the structures were chosen every 200ps. The electrostatic potential of the MDM2 surface was calculated using APBS[7] and Pymol[8]. Figures were generated using Pymol and movies generated using VMD.[9]

In accord with the NMR data,[10] the P27Sm mutant was modeled by adjusting the backbone φ/ψ torsions of the C-terminal residues to a helical conformation followed by regeneration of the side chain orientations. We note here that while the experimental binding affinity data is available for a 19-residue peptide (residues 12-30), the NMR experiments were carried out on a 13-residue fragment (residues 17-29);[10] it is the latter that we have used for our simulations. The crystal structure of the wild type (WT) MDM2-p53 complex shows that residues 19-25 of p53 are α-helical; the NMR data shows an overall increase of helicity in the P27S mutant with a major change at L26, but the experiment did not specify the exact conformation of residues 27-29. We investigate this by modelling two initial conformations of P27S: (i) P27Sc: the backbone conformation of WT p53 is retained; (ii) P27Sm: the C-terminus is modelled as an α-helix; the C-terminus residues L26 and E28 have a propensity for helical conformation.[11]

P27Sc remains stable as modelled (in the WT conformation) during the first 10ns, after which it undergoes conformational transitions to turn, α-helix and pi-helix, particularly at the C-terminal residues and finally stabilizes during the last 3-4ns as a pi-helix (which encompasses the whole peptide ie residues 18-27). This is contrary to the experimental observations which show P27S to be an α-helix. To model P27Sm, we first adjusted the backbone the φ/ψ angles of residues 26-28 to α-helical conformation (ie the peptide is helical from 19-28). However, we observed that during the MD of the uncomplexed state of P27Sm, the α-helical conformation starts to disappear from the C-terminus, propagating quickly to the N-terminus, stabilizing as a pi-helix; this again, like P27Sc, is contrary to the experimental data. Next, the C-terminus of the staring structure of P27Sm was modelled as α-helical only for residues 26-27. Interestingly, we find that residues 19-26 remain α-helical throughout most of the 20ns MD; this result is very similar to that observed by NMR and hence was used for analysis. In

the complexed state we find that both these conformations (of P27Sm) give rise to the same stable conformation (helix across residues 19-28).

To examine the C-terminus of the WT peptide, we remodelled the C-terminal residues (residues 26-28) of p53, both in complexed and uncomplexed states. In both these states, the α-helix at the C-terminus is found to be destabilized by the presence of P27; although the residues 26-28 do not adopt the extended WT conformation, nevertheless they stabilize as a turn. However, the WT peptide is known from spectroscopic studies to adopt an extended C-terminus and so this 'turn' state that we see is only used here as a 'negative control'. Table S2 shows that energetic considerations also screen out this possibility. For the W23L mutant, conformations similar to those used for the final analyses of the WT p53 were used.

Table S1. List of Trajectories each of which has been run for ~18-20ns at 300K, except Trajectory 14 & 15 which have been run for 5ns each.

Trajectory index	System	WT backbone conformation retained at peptide residues	Modeled conformation at peptide residues	Remarks
1	MDM2-p53 (WT), taken from protein data bank (1YCR.pdb)	All	none	used for binding energy calculation
2	MDM2-W23L	All	none	used for binding energy calculation
3	MDM2-P27Sm	17-25	Helix: 26-28 Extended: 29	used for binding energy calculation
4	MDM2-P27Sm	17-25	Helix: 26-27 Extended: 28-29	converges to the same structures as obtained from Trajectory 3. Movie M1e_p27sm2.qt has been shown (other data not shown).
5	MDM2-P27Sc	All	none	used for binding energy calculation
6	MDM2-p53 (hlx)	17-25	Helix: 26-28 Extended: 29	stabilizes as turn at C-terminus
7	Uncomplexed MDM2	Not applicable	Not applicable	used for binding energy calculation
8	Uncomplexed p53	All	None	used for binding energy calculation
9	Uncomplexed p53 (hlx)	17-25	Helix: 26-28 Extended: 29	stabilizes as turn at C-terminus
10	Uncomplexed W23L	All	none	used for binding energy calculation
11	Uncomplexed P27Sm	17-25	Helix: 26-28 Extended: 29	quick transition from α-helix to pi-helix, does not reflect the experimental observation and so not used (data not shown)
12	Uncomplexed P27Sm	17-25	Helix: 26-27 Extended: 29	stable as α-helix, reflects the experimental findings, used for binding energy calculation
13	Uncomplexed P27Sc	All	none	transition from α-helix to pi-helix, does not reflect the experimental data, and not used; binding energy shown in Table S2
14.	Uncomplexed MDM2	Not applicable	Not applicable	snapshot taken from early stage of Trajectory 3 and peptide removed; unliganded MDM2 was simulated
15.	Uncomplexed MDM2	Not applicable	Not applicable	snapshot taken at the end of 20ns of Trajectory 3 and peptide removed; unliganded MDM2 was simulated

Table S2. (a) Components of binding free energy (kcal/mol) for the wild type MDM2-p53 complex.

	MDM2-p53	MDM2	p53	$\Delta_{binding}$
E_{elec}	-1817.0	-1510.8	-103.9	-202.3
E_{vdw}	-378.4	-294.2	-15.3	-68.9
$E_{internal}$	1786.3	1537.2	241.5	7.6
$E_{GBpolar}$	-1728.7	-1556.6	-384.6	212.5
$E_{elec+GBpolar}$	-3545.7	-3067.4	-488.5	10.2
$E_{solv(nonpolar)}$	38.1	34.0	7.6	-3.4
E_{mm} (Total)	-2099.7	-1790.4	-254.7	-54.7
-TS	-1155.3	-1007.3	-186.4	38.4
G				-16.3

Table S2. (b) Components of binding free energy (kcal/mol) for the MDM2-W23L complex.

	MDM2-W23L	MDM2	W23L	$\Delta_{binding}$
E_{elec}	-1982.7	-1510.8	-114.7	-357.3
E_{vdw}	-371.6	-294.2	-20.0	-57.5
$E_{internal}$	1787.0	1537.2	234.9	14.9
$E_{GB\text{-}polar}$	-1588.7	-1556.6	-384.0	351.8
$E_{elec+GB\text{-}polar}$	-3571.5	-3067.4	-498.7	-5.4
$E_{GB\text{-}nonpolar}$	38.1	34.0	7.5	-3.3
E_{mm} (Total)	-2118.0	-1790.4	-276.3	-51.4
-TS	-1152.5	-1007.3	-184.6	39.3
G				-12.1

Table S2. (c) Components of binding free energy (kcal/mol) for the MDM2-P27Sm complex.

	MDM2-P27Sm	MDM2	P27Sm	$\Delta_{binding}$
E_{elec}	-1978.8	-1510.8	-108.8	-359.2
E_{vdw}	-367.9	-294.2	-19.0	-54.7
$E_{internal}$	1782.4	1537.2	227.2	18.1
$E_{GB\text{-}polar}$	-1600.7	-1556.6	-385.4	341.3
$E_{elec+GBpolar}$	-3579.4	-3067.4	-494.2	-17.9
$E_{solv(nonpolar)}$	37.5	34.0	7.4	-3.9
E_{mm} (Total)	-2127.4	-1790.4	-278.7	-58.3
-TS	-1155.7	-1007.3	-185.7	37.3
G				-21.0

***Table S2*.** (d) Components of binding free energy (kcal/mol) for the MDM2-P27Sc complex.

	MDM2-P27Sc	MDM2	P27Sm	$\Delta_{binding}$
E_{elec}	-1869.6	-1510.8	-108.8	-250.0
E_{vdw}	-366.4	-294.2	-19.0	-53.2
$E_{internal}$	1767.3	1537.2	227.2	3.0
$E_{GB\text{-}polar}$	-1694.4	-1556.6	-385.4	247.5
$E_{elec+GB\text{-}polar}$	-3564.0	-3067.4	-494.2	-2.5
$E_{GB\text{-}nonpolar}$	38.6	34.0	7.4	-2.8
E_{mm} (Total)	-2124.6	-1790.4	-278.7	-55.5
-TS	-1158.0	-1007.3	-185.7	35.0
G				-20.5

Table S2. (e) Components of binding free energy (kcal/mol) for the MDM2-P27Sc complex using the P27Sc trajectory for the uncomplexed state.

	MDM2-P27Sc	MDM2	P27Sc	$\Delta_{binding}$
E_{elec}	-1869.6	-1510.8	-161.1	-197.7
E_{vdw}	-366.4	-294.2	-22.0	-50.2
$E_{internal}$	1767.3	1537.2	228.0	2.1
$E_{GB\text{-}polar}$	-1694.4	-1556.6	-342.4	204.6
$E_{elec+GB\text{-}polar}$	-3564.0	-3067.4	-503.5	6.9
$E_{GB\text{-}nonpolar}$	38.6	34.0	6.8	-2.2
E_{mm} (Total)	-2124.6	-1790.4	-290.7	-43.5
-TS	-1158.0	-1007.3	-182.9	32.2
G				-11.3

Table S2. (f) Components of binding free energy (kcal/mol) for the MDM2-P27Sm complex using the P27Sc trajectory for the uncomplexed state.

	MDM2-P27Sm	MDM2	P27Sc	$\Delta_{binding}$
E_{elec}	-1978.8	-1510.8	-161.1	-306.9
E_{vdw}	-367.9	-294.2	-22.0	-51.6
$E_{internal}$	1782.4	1537.2	228.0	17.2
$E_{GB\text{-}polar}$	-1600.7	-1556.6	-342.4	298.4
$E_{elec+GB\text{-}polar}$	-3579.4	-3067.4	-503.5	-8.5
$E_{GB\text{-}nonpolar}$	37.5	34.0	6.8	-3.3
E_{mm} (Total)	-2127.4	-1790.4	-290.7	-46.3
-TS	-1155.7	-1007.3	-182.9	34.5
G				-11.8

Table S2. (g) Components of binding free energy (kcal/mol) for the MDM2-p53 complex where the simulation of the complex started with a modeled helix at the C-terminus of the peptide.

	MDM2-p53(hlx)	MDM2	p53	$\Delta_{binding}$
E_{elec}	-1757.5	-1510.8	-103.9	-142.8
E_{vdw}	-379.2	-294.2	-15.3	-69.7
$E_{internal}$	1784.8	1537.2	241.5	6.1
$E_{GBpolar}$	-1785.2	-1556.6	-384.6	156
$E_{elec+GBpolar}$		-3067.4	-488.5	13.2
$E_{solv(nonpolar)}$	38.2	34.0	7.6	-3.4
E_{mm} (Total)	-2098.9	-1790.4	-254.7	-53.8
-TS	-1152.8	-1007.3	-186.4	40.9
G				-12.9

Table S2. (h) Components of binding free energy (kcal/mol) for the MDM2-p53 complex where the complexed and uncomplexed states of the peptide started from the modeled helix at the C-terminus.

	MDM2-p53(hlx)	MDM2	p53(hlx)	$\Delta_{binding}$
E_{elec}	-1757.5	-1510.8	-124.1	-122.6
E_{vdw}	-379.2	-294.2	-18.1	-66.9
$E_{internal}$	1784.8	1537.2	249.2	-1.6
$E_{GBpolar}$	-1785.2	-1556.6	-371.2	142.6
$E_{elec+GBpolar}$	-3542.7	-3067.4	-495.3	20
$E_{solv(nonpolar)}$	38.2	34.0	7.2	-3.0
E_{mm} (Total)	-2098.9	-1790.4	-257.0	-51.5
-TS	-1152.8	-1007.3	184.3	38.8
G				-12.7

***Table S2*.** (i) Components of gas phase energies of MDM2 extracted from different complexes as well as from the unliganded state. The entropic stabilization of MDM2-P27Sc is characterized by loss of van der Waals and electrostatic interactions in MDM2; the enthalpic stabilization of MDM2-P27Sm complex is characterized by gain in electrostatic interactions.

	MDM2 (Unliganded Trajectory)	MDM2 taken from the complexes			
		W23L	WT	P27Sm	P27Sc
E_{elec}	-1510.8	-1538.3	-1398.0	-1588.4	-1390.2
E_{vdw}	-294.2	-294.3	-302.1	-294.5	-291.1
$E_{elec}+ E_{vdw}$	-1805.0	-1832.6	-1700.1	-1882.9	-1681.3
$E_{internal}$	1537.2	1547.4	1540.9	1552.9	1536.9

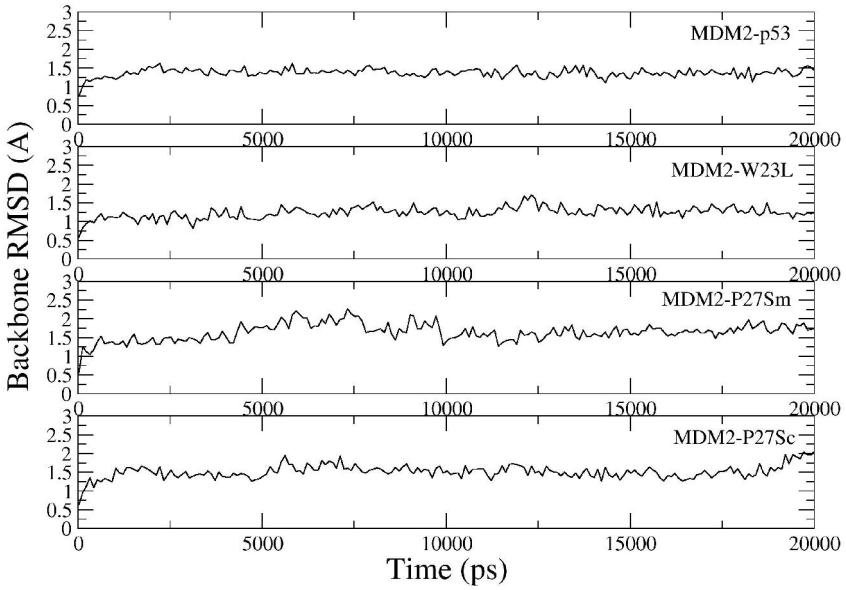

Figure S1. (a) Backbone root mean square deviation (RMSD) of the complexes as a function of time (along 20ns trajectory). For each case the energy minimized starting structure was taken as reference. Stability of plots reflects stability of simulations.

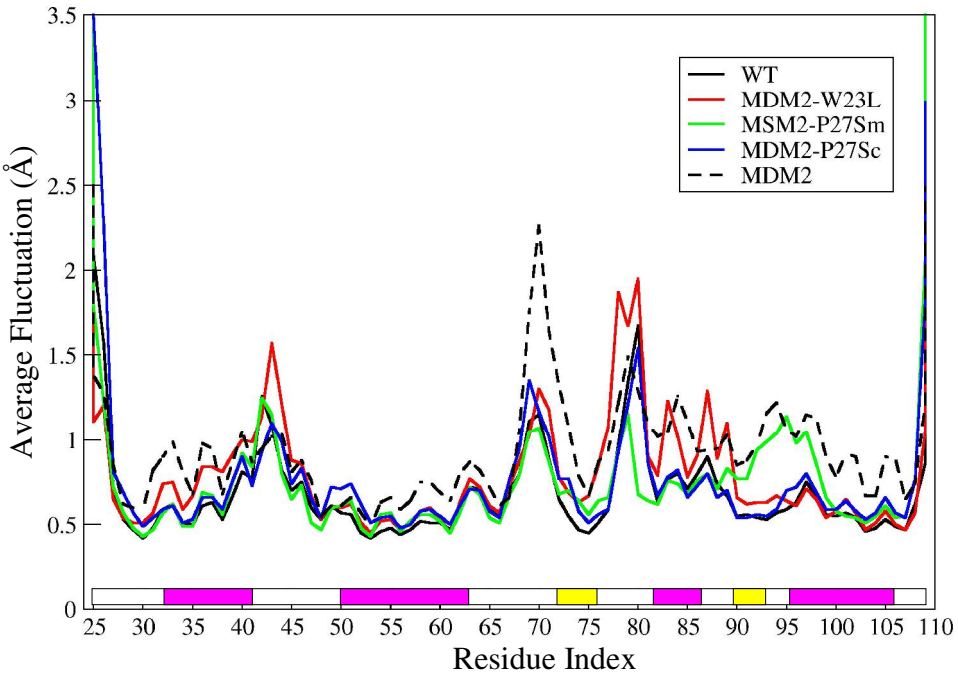

Figure S1. (b) Fluctuation of C_α atoms of MDM2 averaged over the last 10ns of the trajectory. Data are shown for the uncomplexed MDM2 (dashed line) and MDM2 complexed (solid line) with different peptides. Secondary structures are labeled with colors: purple (α-helix), yellow (β-strand). The uncomplexed MDM2 (dashed line) shows higher fluctuations and narrowing of the peptide binding cleft, in agreement with data from other simulations;[12] (also see Figure S4h below) and from experiments.[13] The mutation W23L causes a loss of hydrophobic packing in the complexed state and this, in a concerted manner, affects different regions of MDM2 including high mobility in residues 32-46 and 73-94. In P27Sm, mobility increases selectively around the C-terminus of the MDM2, in residues 90-98 and in the loop region containing H96. These observations are in accord with experimental findings that the MDM2 binding cleft adapts itself to accommodate a diversity of ligands.[13,14,15] Indeed, we find that in addition to the length of the peptide modulating the mobility of MDM2 as has been reported experimentally,[14] the amino acid composition of the peptide can also influence the mobility of MDM2 in diverse ways, in particular in the region of the peptide binding cleft (see below).

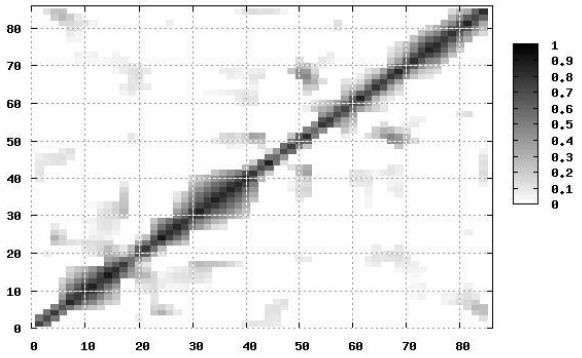

MDM2-p53

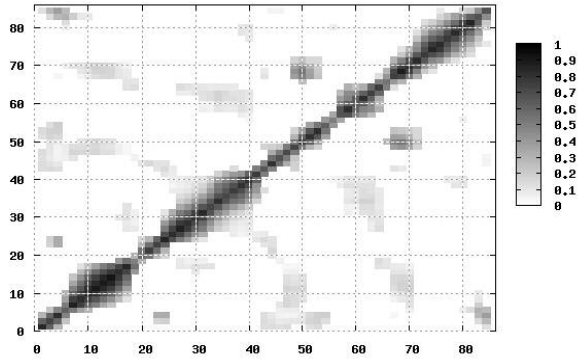

MDM2-W23L

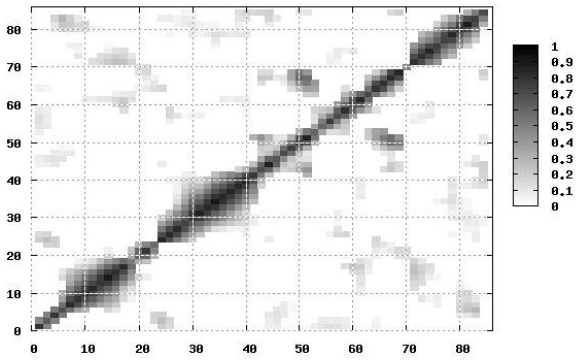

MDM2-P27Sm

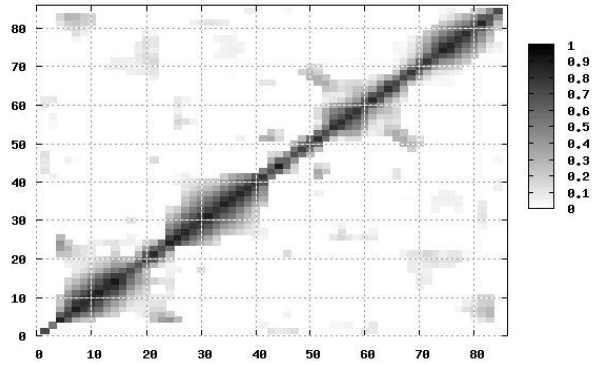

MDM2-P27Sc

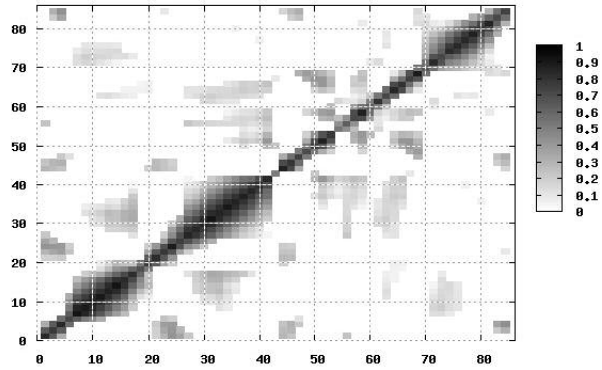

MDM2 uncomplexed

Figure S1. (c) Plot of covariance matrices of C_α-atoms of MDM2 in complexed and uncomplexed state. The numbers in the axes indicate the residue index. The plots again show that changes do take place in the global dynamics upon complexation of peptide variants.

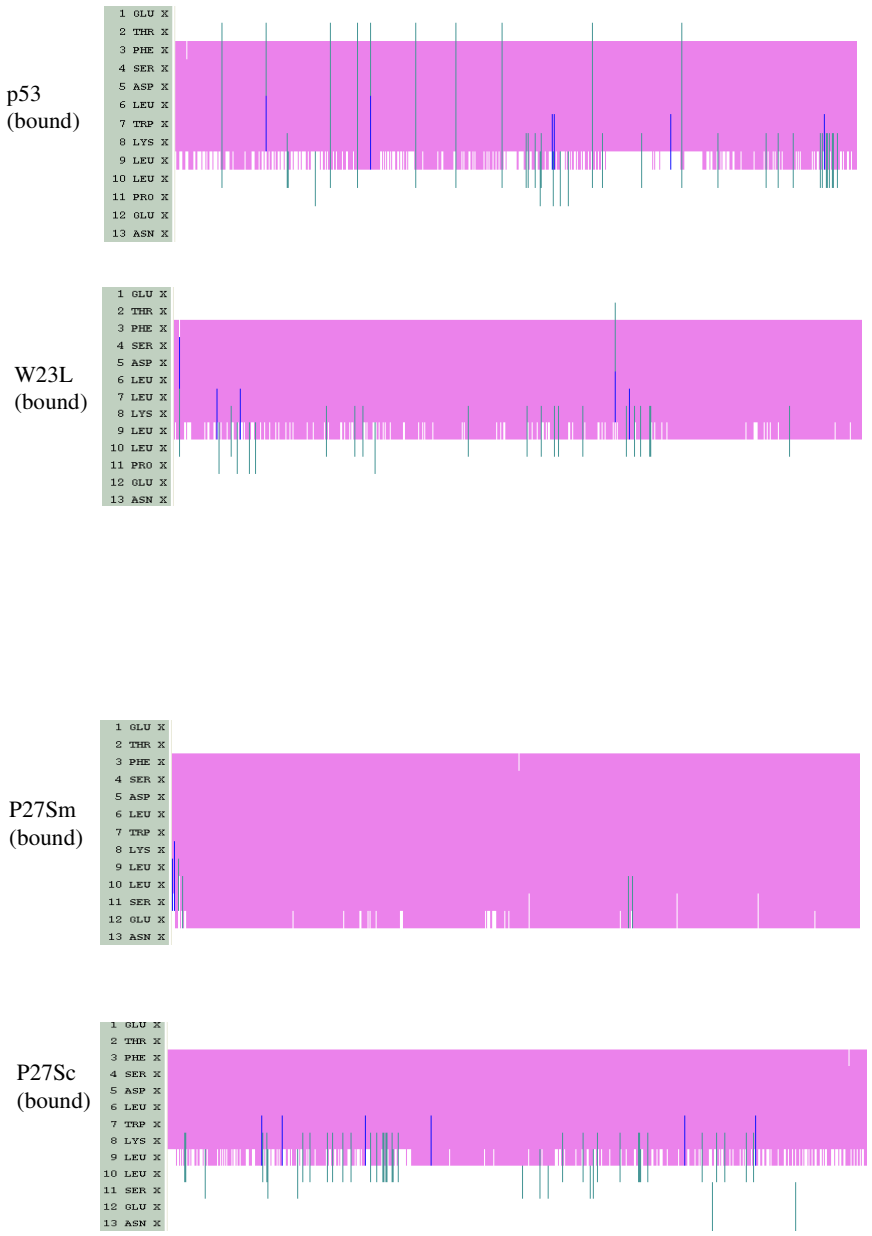

Figure S2. (a) Secondary structure of the complexed peptides along the 20ns trajectories. The index of the residues in the figures are renumbered such that residue '1 Glu' correspond to E17 (of the crystal structure 1YCR). Secondary structures are colored as follows: alpha helix (purple), 3_{10}-helix (blue), pi-helix(red), turn (green), random coil (white).

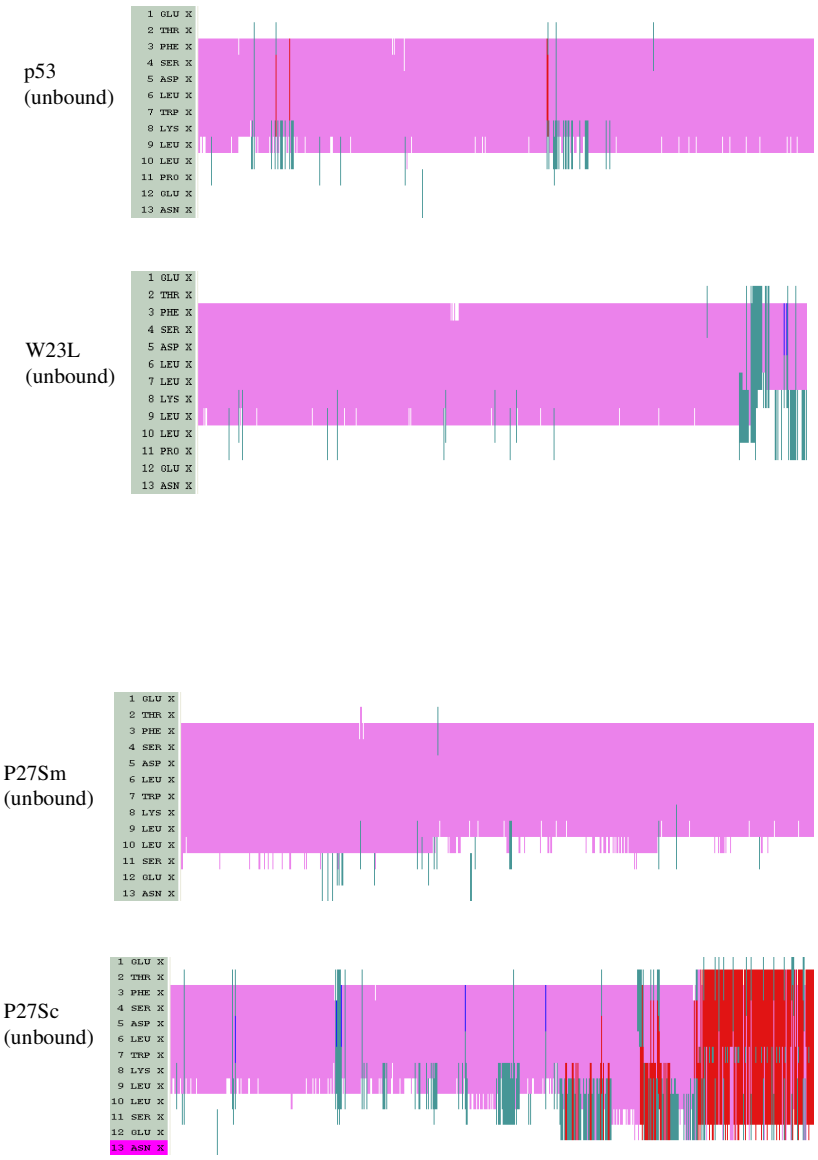

Figure S2. (b) Secondary structure plot for the uncomplexed peptides along 20ns trajectories. The residue numbering and the coloring scheme are the same as in Figure S2(a). The uncomplexed state of P27Sc converges to a pi-helix; the P27Sm remains stable as a helix and is in agreement with the experimental observations of Zondlo *et al.*[10] (see text).

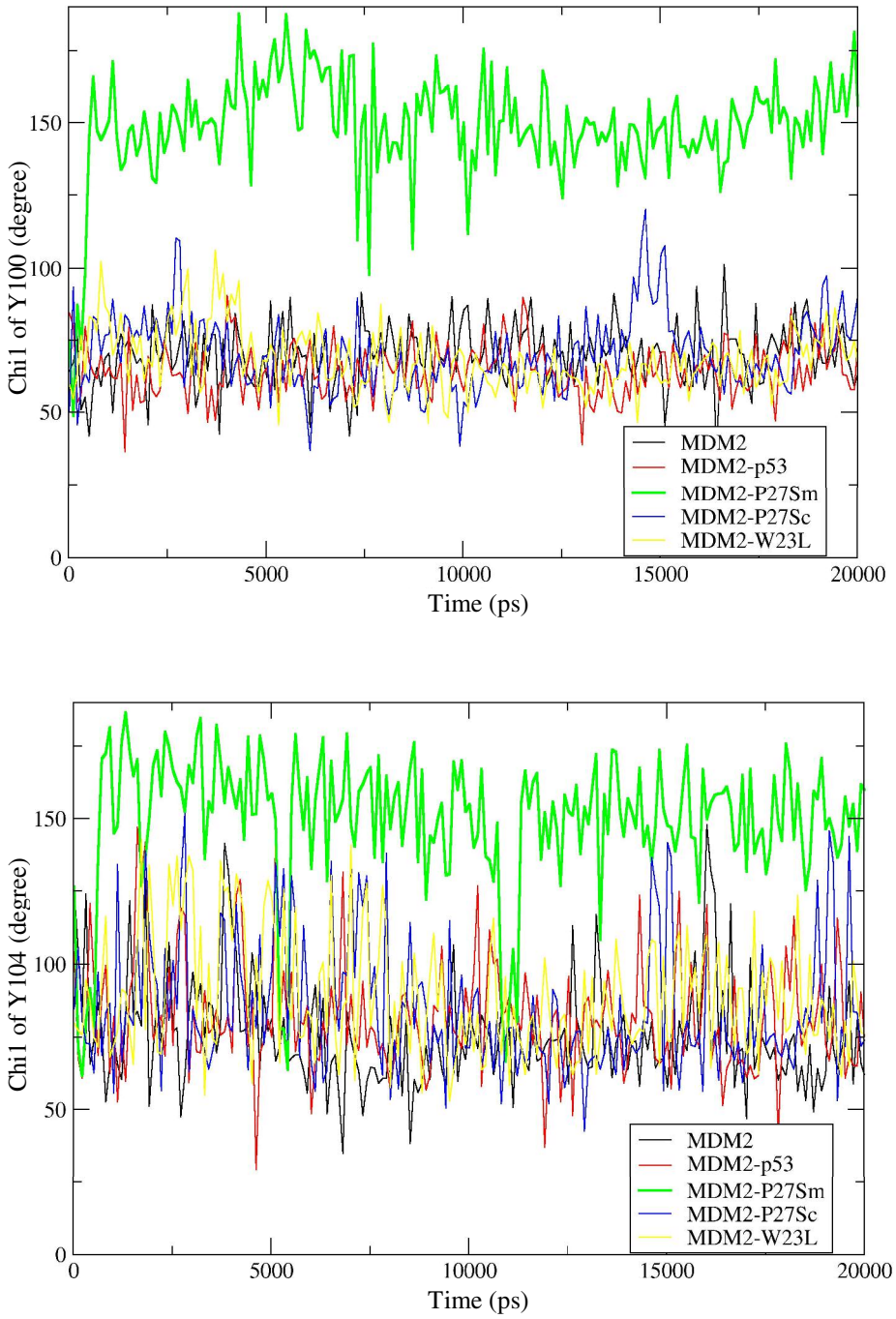

Figure S3. (a) Chi1 (χ1) angle of Y100 and Y104 of MDM2 as a function of time. Data has been shown for MDM2 in the uncomplexed state as well as in the complexed state. A clear flip in Y100 and Y104 is seen in the case of MDM2-P27Sm (green line). In the case of the other peptides, the extended C-terminus prevents the flip from occurring. In the case of uncomplexed MDM2, the narrowing of the cleft prevents the Y from flipping.

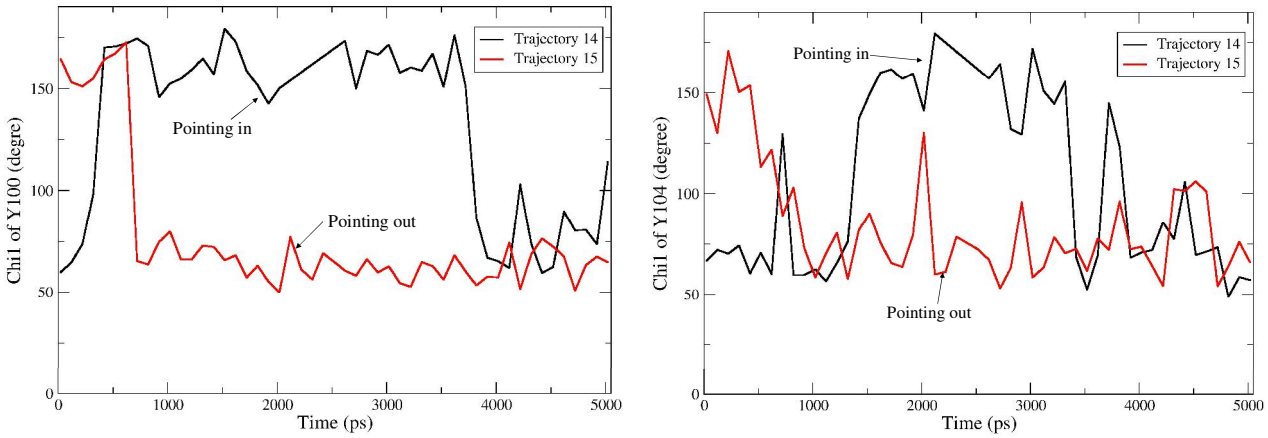

Figure S3. (b) Chi1 (χ1) angle of Y100 and Y104 residues of uncomplexed MDM2 as a function of time. Data taken from Trajectory 14 and 15 (referred to in Table S1).

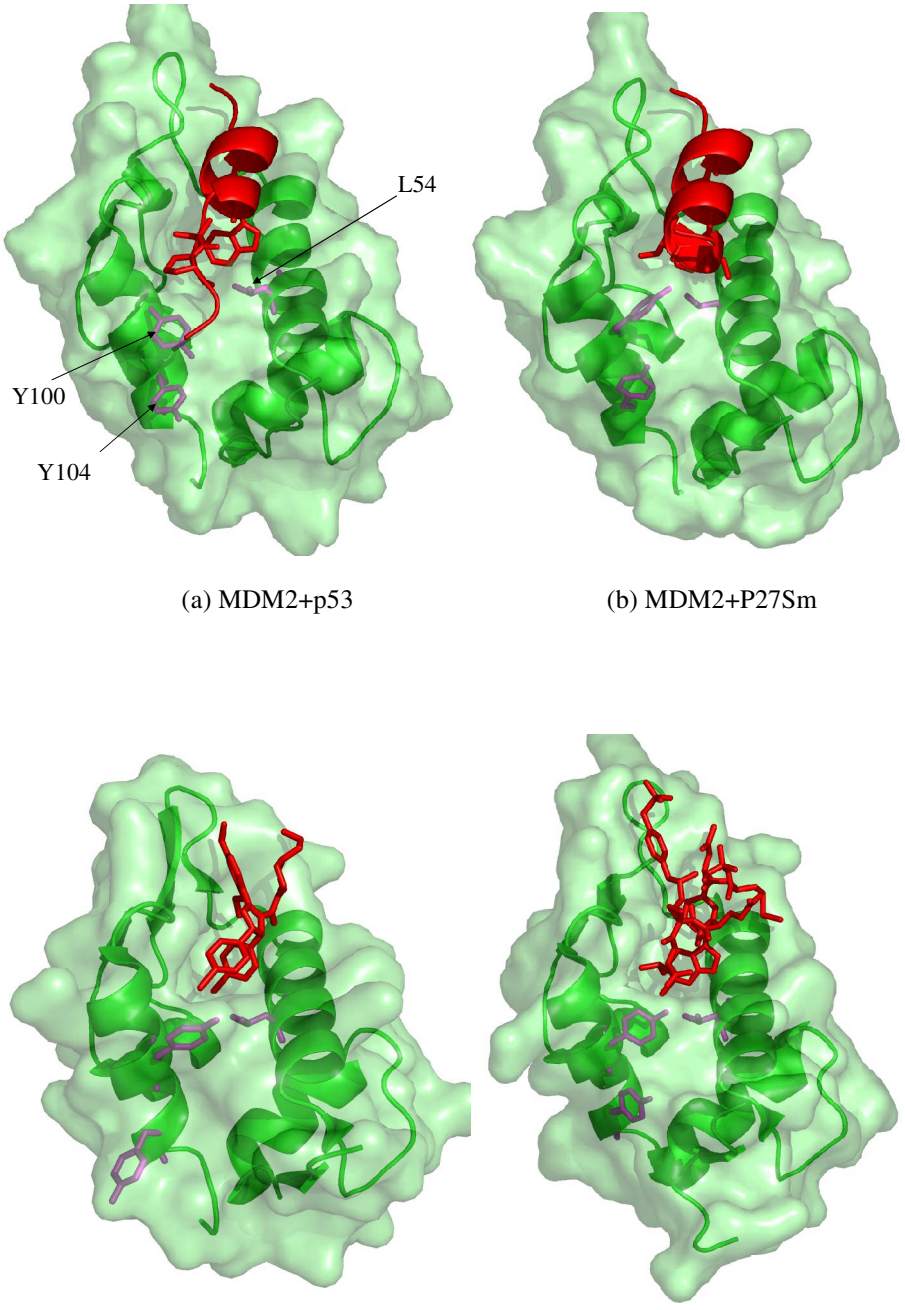

(a) MDM2+p53 (b) MDM2+P27Sm

(c) MDM2+nutlin (1RV1) (d) MDM2+8 residue peptide (2GV2)

Figure S4. (a)-(b) WT and MDM2-P27Sm complexes: snapshots taken at the end of 20ns MD. (c)-(d) structure of MDM2 (green cartoon+surface) with two different ligands (red) taken from the protein data bank (PDB) with PDB codes in parentheses[16,17]; Y100/104 and some other important side chains are shown in purple sticks.

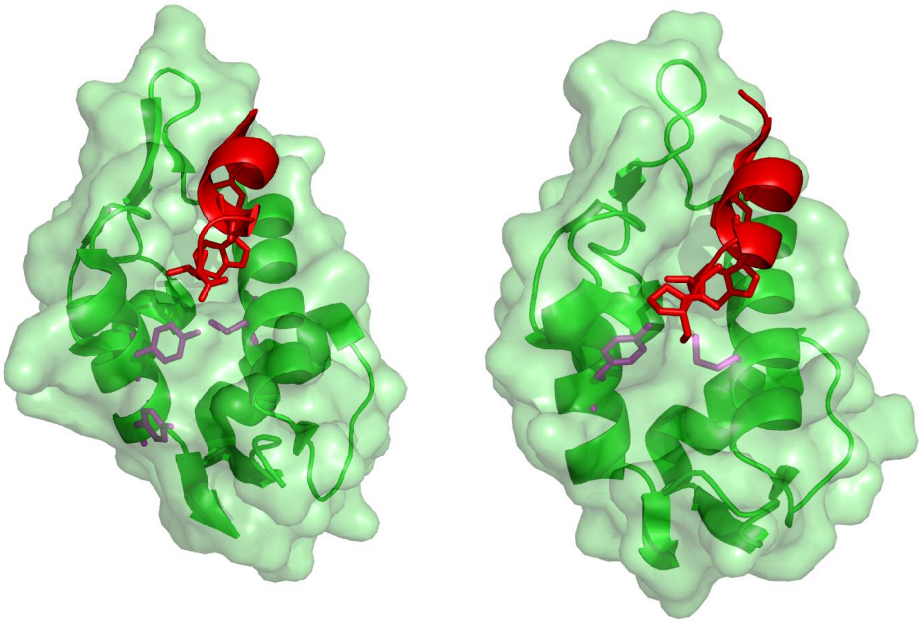

(e) MDM2+optimized peptide (1T4F) (f) MDMX+p53 (2Z5T)

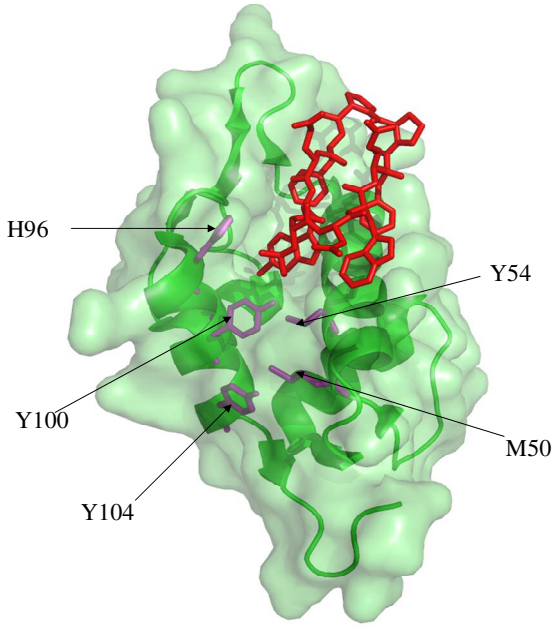

(g) MDM2+beta hairpin peptide (2AXI)

Figure S4. (e)-(g) MDM2 and MDMX (green cartoon + surface) with different ligands (red). The structures are taken from protein data bank (PDB) with PDB codes in parentheses[18,19,20]; Y100/104 (Y96 in MDMX) and some other important side chains are shown in purple stick.

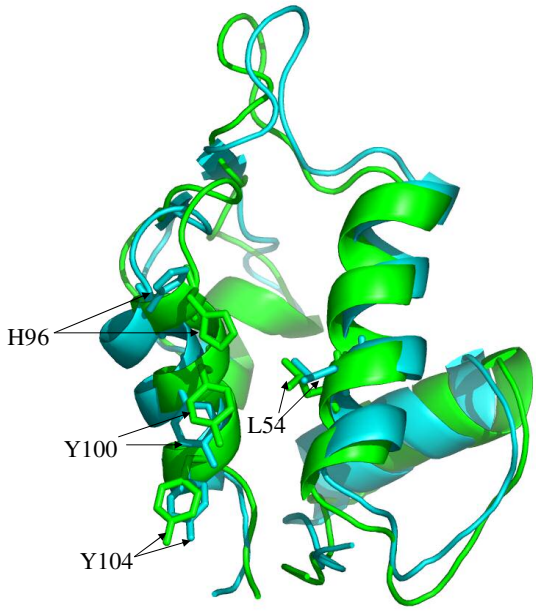

(h) Uncomplexed (green) and complexed (cyan) MDM2

Figure S4. (h) Structures of complexed and uncomplexed MDM2 superposed to show changes in overall topology (structures taken at the end of 20ns MD).

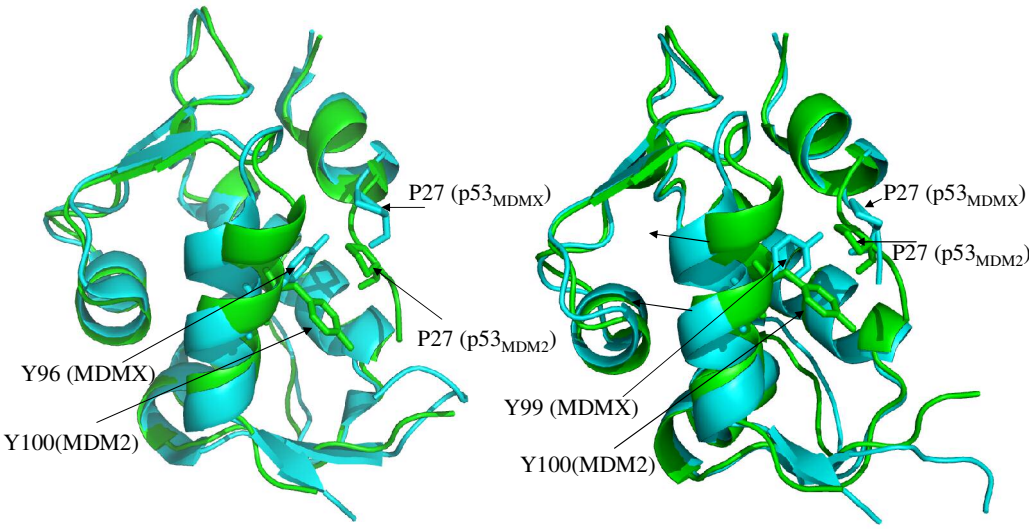

(i) MDM2-p53 (green), MDMX-p53[zebrafish] (cyan)

(j) MDM2-p53 (green), MDMX-p53 [Human] (cyan)

Figure S4. Superimposed crystal structures of (i) MDM2-p53 in green (1YCR)[1] and MDMX-p53 (zebrafish MDMX with humanized binding site residues) in cyan (2Z5T)[19] and (j) MDM2-p53 in green (1YCR)[1] and MDMX-p53 (human MDMX)[21] in cyan (structure kindly provided by Prof. Tad Holak), indicating residue Y100 (or its equivalent Y96/Y99). The differences of orientations of Y100/96/99 seem to be determined by P27. The packing of P27 against the MDM2 surface in MDM2-p53 does not allow Y100 to move while in MDMX, the larger distance between Y96/99 and P27 (P27 has moved away from the surface) creates space for the Y96/99 to flip in towards the binding cavity.

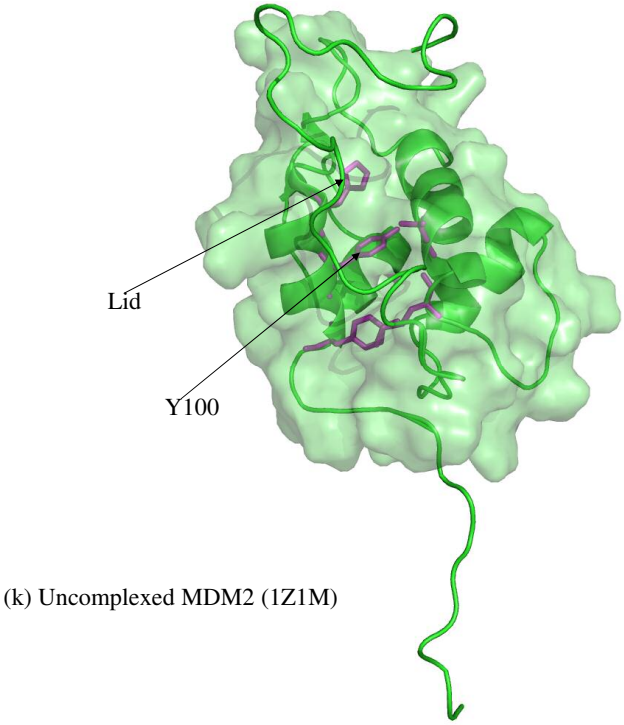

(k) Uncomplexed MDM2 (1Z1M)

Figure S4. (k) Representative snapshot of uncomplexed MDM2 determined by NMR[13] with PDB codes in parentheses. The surface of MDM2 has been shown for residues 25-109 to show that the lid region (residues 1-24) interacts with the surface near the binding cavity and Y100 points towards the binding pocket.

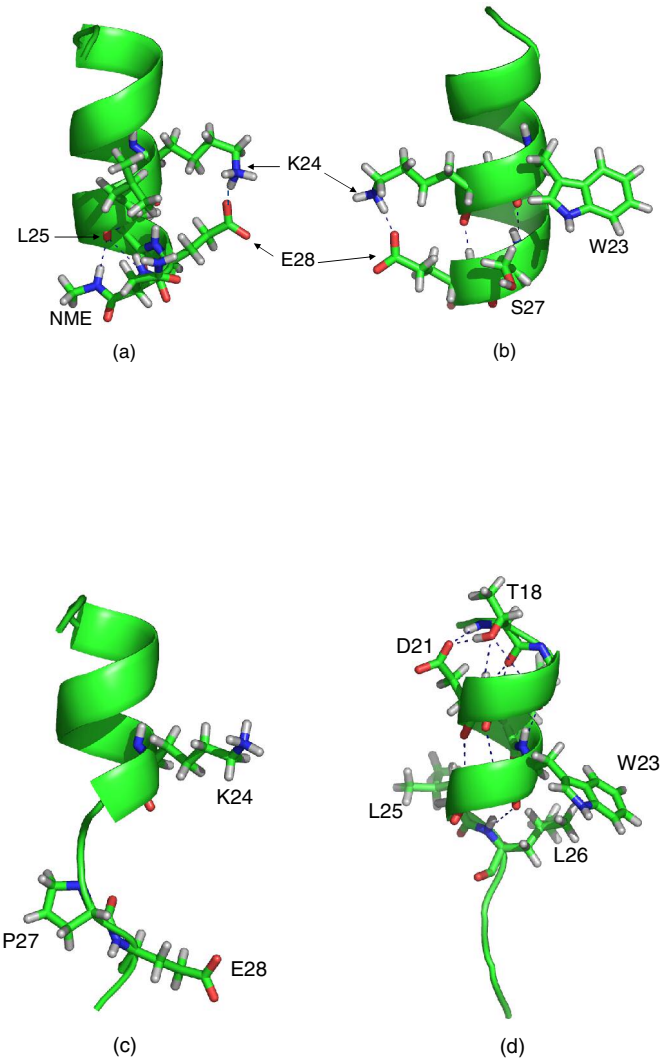

Figure S5. Example of intra-helix H-bonds and salt bridge interactions in the peptides: (a) & (b) P27Sm in the complexed state (two different orientations) showing the proximity of K24 and E28 (~3.7 Å) allowing for the formation of a salt bridge (c) wild type p53 (complexed with MDM2) shows the impossibility of salt bridge formation between K24 and E28 with an 11Å separation between the two (d) example of intra-helical H-bonds of WT p53 complexed to MDM2. The salt bridge is not formed in the W23L and P27Sc in the complexed state as they have backbone conformations similar to that of WT.

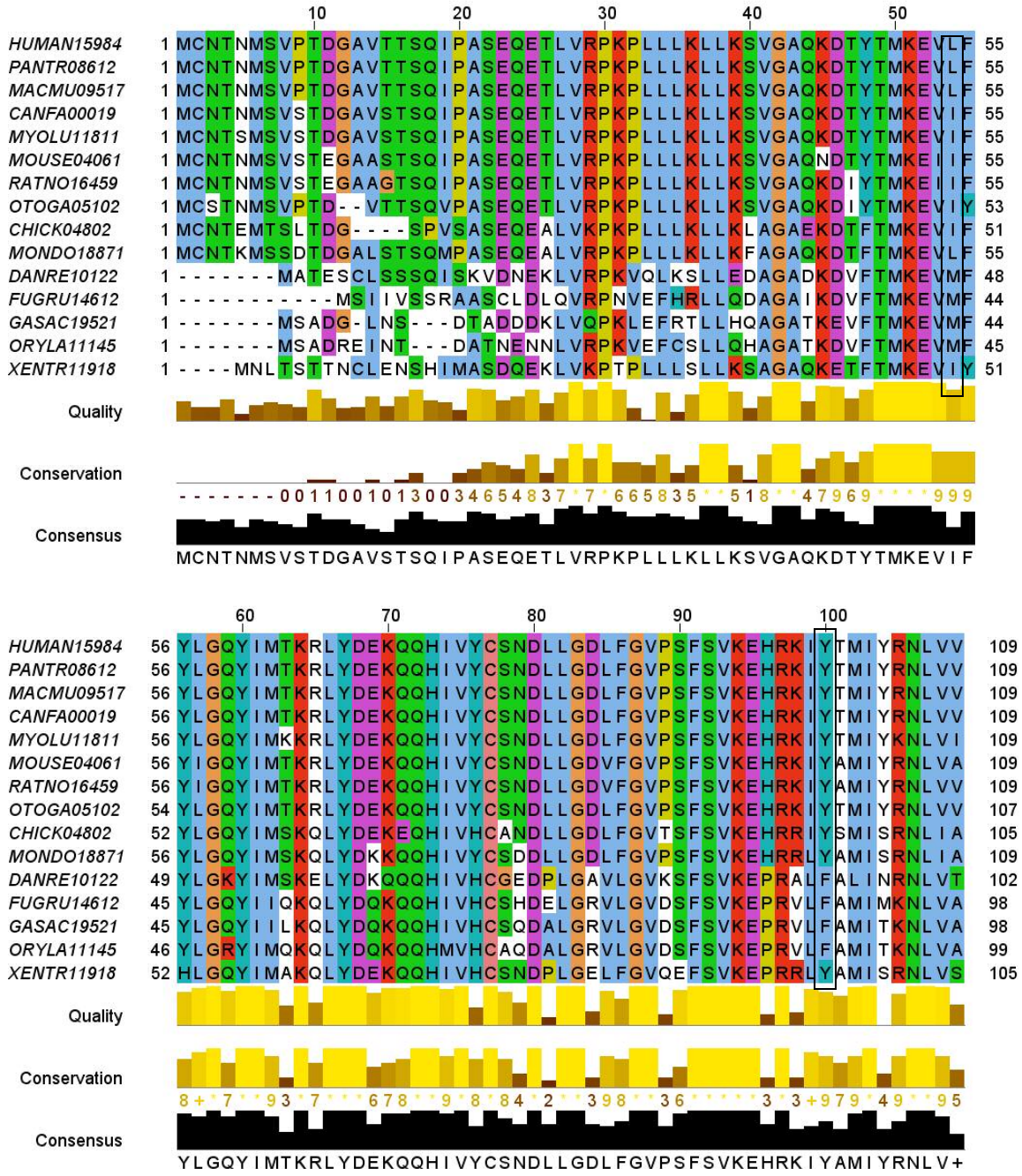

Figure S6. Sequence alignment of the MDM2 across different species. Note the conservation of boxed residues Y100 and L54 (this position seems to have long chain hydrophobic residues such as L, I, M). The alignment was done using the webserver at http://omabrowser.org[22] and the figure was generated using Jalview.

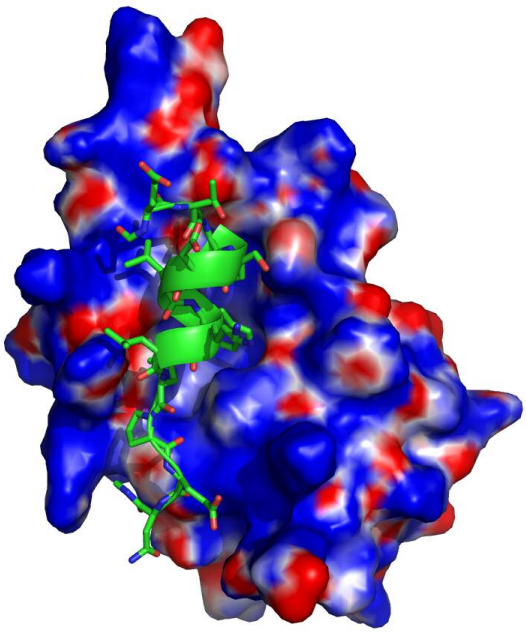

(a) Wild type MDM2-p53

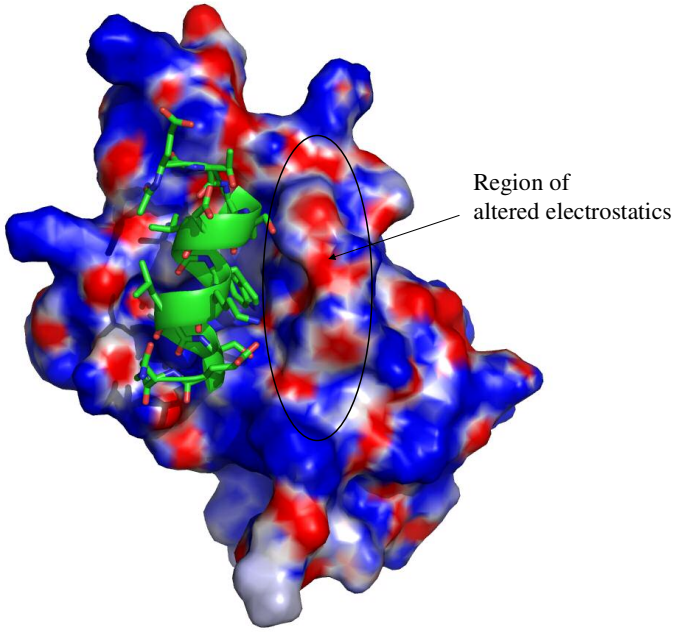

(b) MDM2-P27Sm

Figure S7. Electrostatic potential mapped on the MDM2 surface for (a) MDM2-p53 and (b) MDM2-P27Sm complexes computed using APBS[7] and Pymol[8]. The color scale is red (-5 kT/e) to blue (+5 kT/e). The closure of the cleft wall in MDM2 around P27Sm is evident leading to (a) a 'cosier' fit; (b) altered electrostatics along the 51-62 cleft region that we are currently utilizing to design peptides with a higher affinity for MDM2.

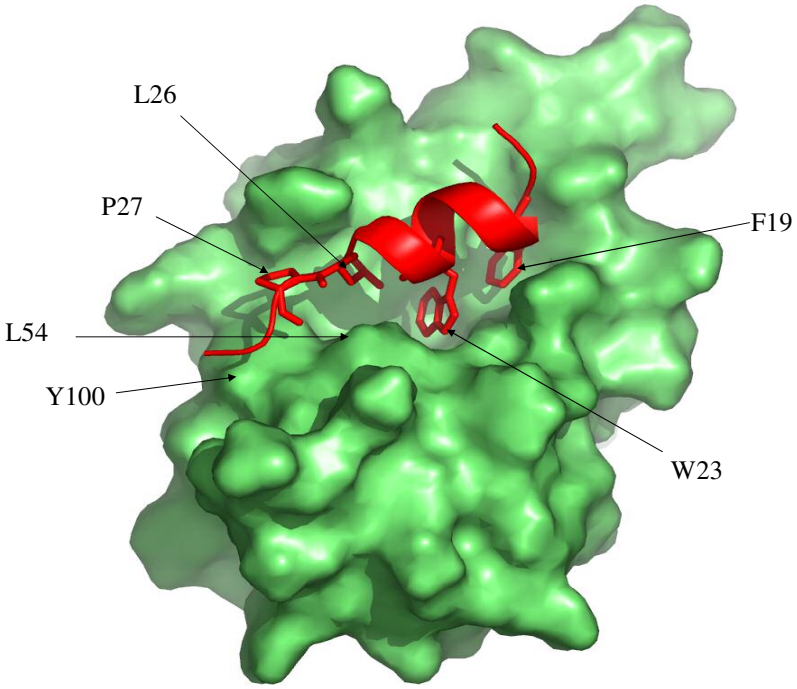

Figure S8. (a) Larger view of Figure 1a: the WT complex.

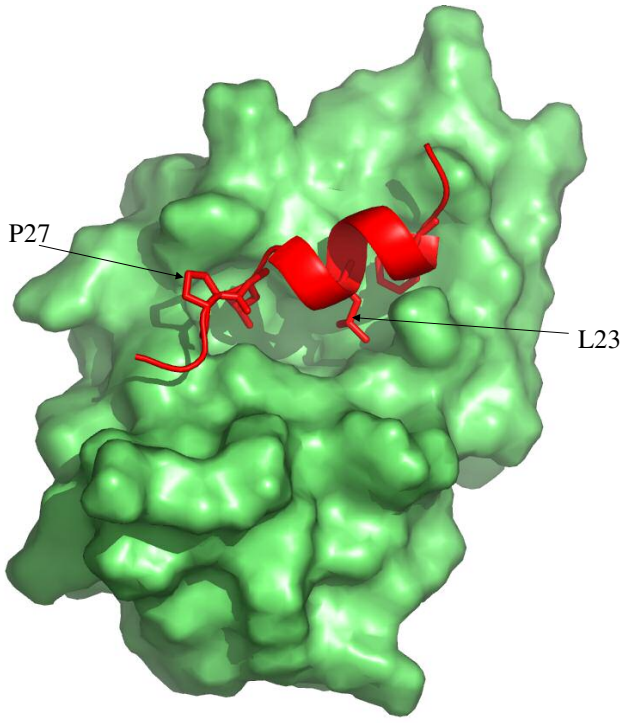

Figure S8. (b) Larger view of Figure 1b: MDM2-W23L complex.

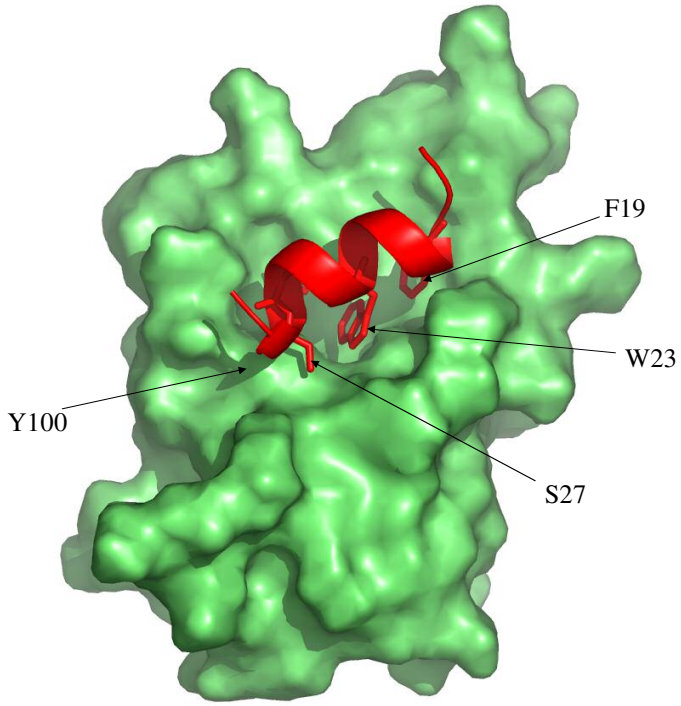

Figure S8. (c) Larger view of Figure 1c: MDM2-P27Sm

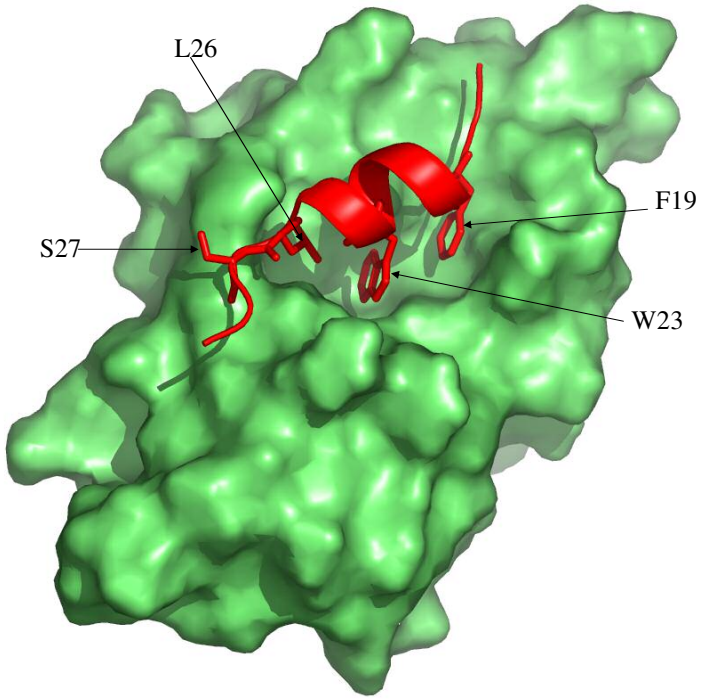

Figure S8. (d) Larger view of Figure 1d: MDM2-P27Sc

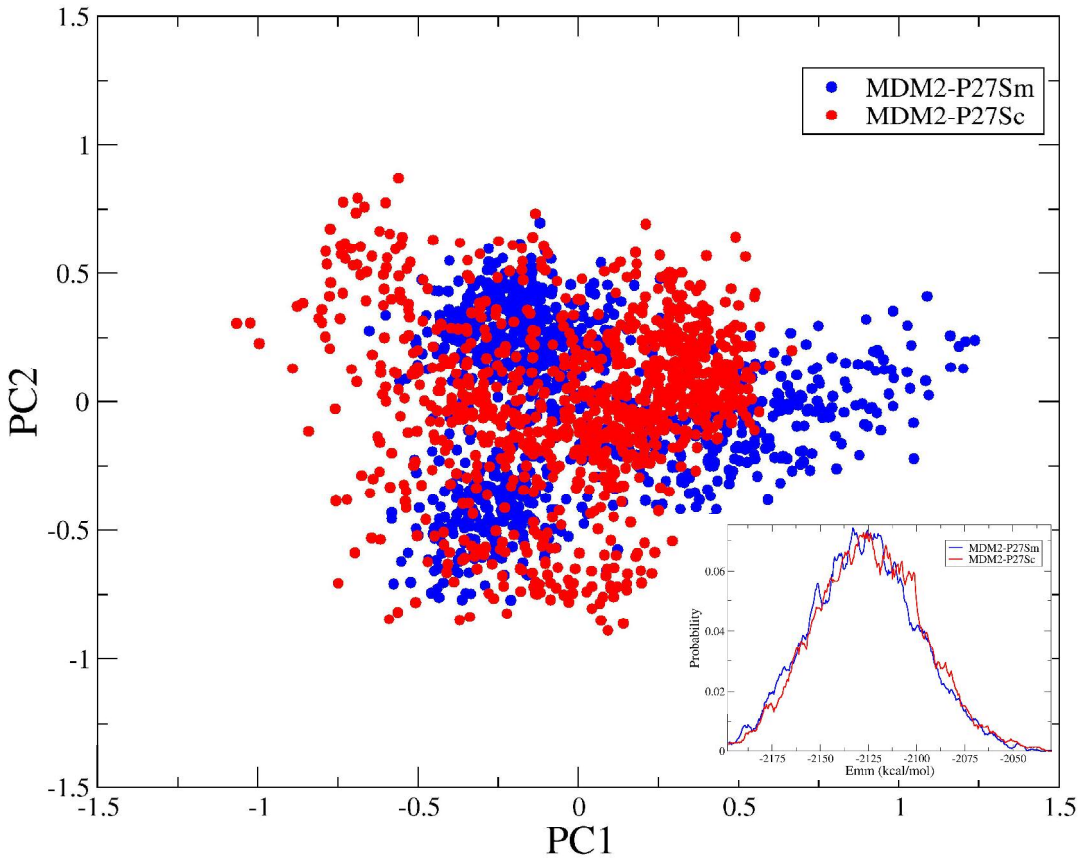

Figure 9. Plot of projection of 20ns trajectories of MDM2-P27Sm (blue) and MDM2-P27Sc (red) complexes along first two principal components (PC1 vs. PC2). (***Inset***) probability distribution of E_{mm} (total) of the two complexes.

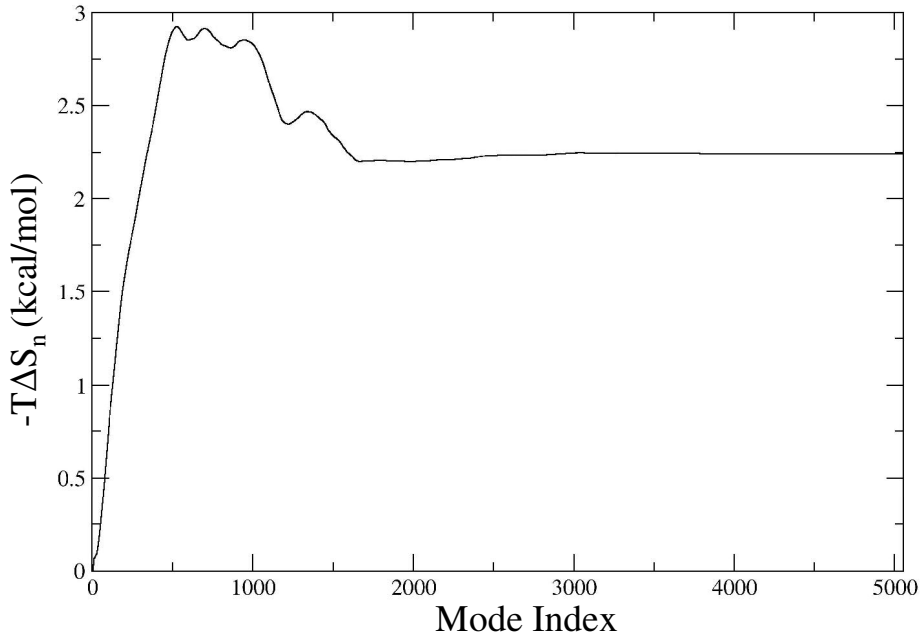

Figure S10. (a) Plot of difference of cumulative entropic contribution (-T ΔS_n) as a function of normal mode. The entropic contribution of i'th mode of vibration was computed using the following expression $S_i' = (h\nu_i / T)/(e^{h\nu_i / kT} - 1) - k\ln(1 - e^{-h\nu_i / kT})$;[23,24] The cumulative sum of the vibrational entropy of the system upto n'th mode is calculated as $S_n = \sum_{i=1}^{n} S_i'$; and the difference of S_n for MDM2-P27Sc and MDM2-P27Sm complexes are calculated as, $\Delta S_n = S_n(P27Sc) - S_n(P27Sm)$, '-$T\Delta S_n$' has been plotted as a function of n (normal mode index).

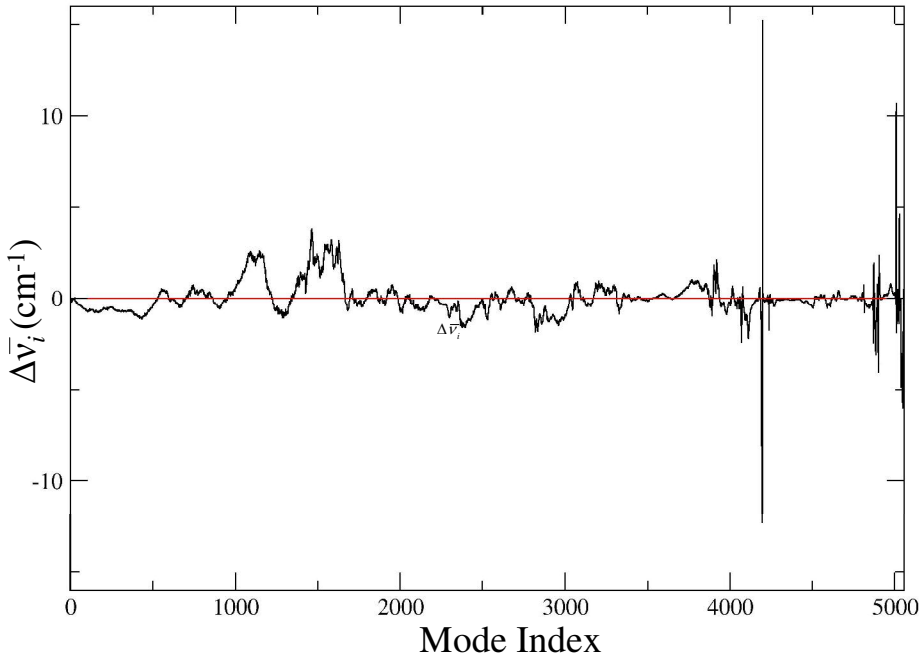

Figure S10. (b) Plot of the differences of frequency (averaged over multiple snap shots) of each normal modes. For each complex the frequency of the i'th vibrational mode has been averaged over the different snapshots and the difference average frequency of the i'th mode's frequency of two complexes have been calculated as $\Delta\bar{\nu}_i = \bar{\nu}_i(P27Sc) - \bar{\nu}_i(P27Sm)$. The initial trend of the values of $\Delta\bar{\nu}_i$ at lower modes clearly shows that there is a red-shift of the overall vibration of the P27Sc complex at the lower frequency range.

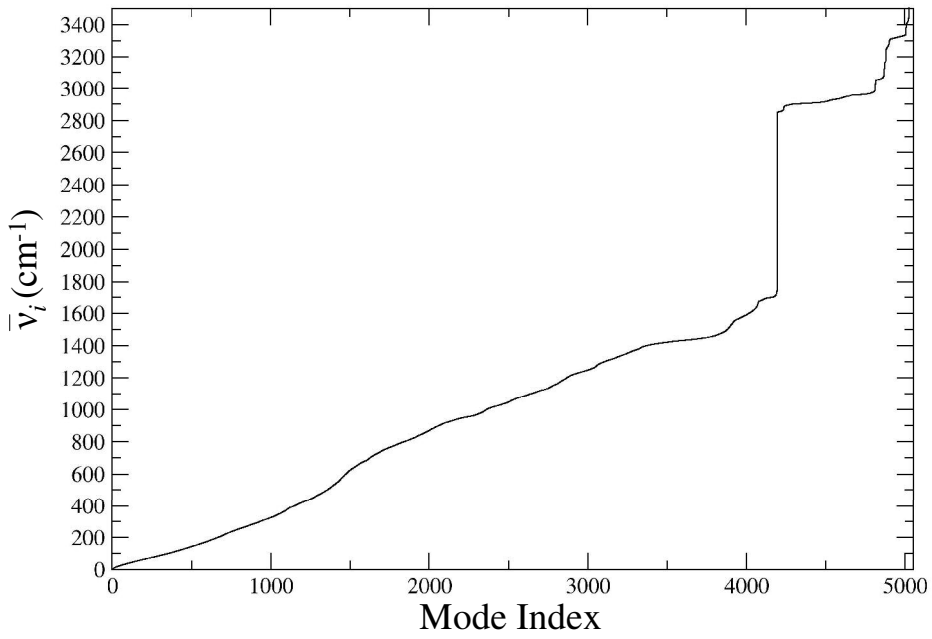

Figure S10. (c) Plot of frequency ($\bar{\nu}_i$) of normal modes as a function of mode index of MDM2-P27Sc complex.

Notes on induced fit vs. preorganization: We examined the distributions of conformations of the peptides and MDM2 when free and when complexed, to estimate the fractions that exist in a near-bound mode (i.e. those that are preorganized to maximize binding), and the fractions that become organized (or are induced to) upon binding. For MDM2, we focused on Y100 whose dynamics clearly modulate optimal binding.

During the uncomplexed state, we know that P27S exists in a helical conformation (this is the experimental data[10] that we have used in our simulations). In its uncomplexed state, we have already seen that MDM2 is characterized by Y100 that is oriented away from the cavity ('out' during the entire 20ns of the simulation (Figure S3a). In contrast, the complete ensemble of structures derived using NMR[13] show the Y100 to point into the cavity ('in'); however, upon closer inspection of the NMR structures (Figure S4j), it becomes clear that this conformation is forced as a result of the contacts formed by the residues that form the flexible lid-region of MDM2 which has been excluded in our study. This was done because the peptide binding experiments[10] that are being examined in our current study, involve MDM2 with this lid region removed (MDM2 used was from residues 25-117).

To test the dynamics of Y100 further, we have now carried out an additional two simulations (5ns each) of unliganded MDM2 starting from the two extreme conformations of Y100 – one with Y100 'in' and one with Y100 'out'. Both these starting structures were taken from the trajectory of the MDM2-P27Sm complex (Trajectory 3 of Table S1). The first structure was taken from the beginning of the simulation as the Y100 was 'out' (Trajectory 14, we refer to this as simulation T14), as in the p53-MDM2 crystal structure. The second structure was taken at the end of 20ns of the simulation of Trajectory 3, when Y100 was pointing 'in' (Trajectory 15, we refer to this as simulation T15). In T14, Y100 starts from the 'out' position and flips 'in' within 1ns where it remains stable for the next 3ns and then flips 'out'. In contrast, in T15, Y100 starts from the 'in' position and flips 'out' within 1ns and then remains stable for the next 4ns (Figure S3b). This suggests that although MDM2 in its apo state predominantly exists with Y100 in the 'out' state, a fraction of MDM2 does exist with Y100 flipped 'in'.

In the complexed state, when the peptide is in an extended conformation (as is the case for WT, W23L, P27Sc) Y100 is constrained to remain 'out'. If however, the peptide is helical (P27Sm), Y100 is induced to the 'in' state through rapid rearrangement of residues local to Y100 and, this event occurs within a few 100 ps (the simulations had started with Y100 'out'). Distributions of the two states in the conformational space are very similar, as evidenced by principal component analysis (Figure S9) which shows great overlap. Energetically, the distributions of the enthalpies of the two states are also very similar (Figure 9, inset) and again suggest broadly similar populations. The difference between the

overall free energies (0.5kcal/mol) also suggests that the difference in the ground state populations (of the complexed states) will be approximately 2-fold in favour of the helical states. The reason why we do not see interconversions between the two states was revealed by reaction path calculations (data not shown) which suggest very high enthalpic barriers (~90 kcal/mol) to this process which puts them beyond the simulated timescales.

To further explore the conformational constraints of the peptide, we carried out a separate simulation (trajectory no 4 in Table S1), where we changed the conformation of the P27S peptide such that only residues 26 and 27 were helical (in contrast to P27Sm where residues 26-28 were modeled as helical). During the simulation (movie M1e_P27Sm2.qt) it is clear that this peptide now samples both conformations – near helical and extended – and is well correlated with the motion of Y100. When the peptide is helical, Y100 points 'in' and when the peptide is extended, Y100 flips 'out'.

These findings unequivocally suggest that MDM2 (without the lid region) is largely preorganized to bind peptides that exist in extended conformations; however local flexibility also enables rapid reorganization (induction) into conformations that would optimize interactions with other conformations of peptides, such as helical ones, or indeed, small molecules such as nutlins. We of course cannot witness such events during our simulations as the timescales involved are much larger. This suggests that evolutionarily, this local flexibility may have evolved to fine-tune interactions with p53 giving it a broader range of binding affinities depending upon the biological context. This makes sense biologically as it is important that p53 rapidly binds MDM2, gets modified, and is quickly cleared through the degradation pathway.

Notes on components of the binding energy: It is interesting that for the single residue change from P to S at position 27, when the conformations of the peptides are extended, the increase in ground state enthalpy is very small (~kT). However, when the conformation of the mutant peptide is helical, then the associated enthalpic gain is 6kT. Despite a large loss of contacts between the peptide and protein that result from mutating P to S (similar loss of van der Waals energies in both states of the mutant), the electrostatic gain is roughly 25-75% in the mutant states. This arises from the increased polar character of the S peptide, its ability to form H-bonds (both within the peptide and with the protein – either direct of through water molecules) and the rearrangement of local residues such as L54, H96 and Y100 that lead to 'cosier' packing in the helical states. Indeed, this results in higher strain in P27Sm relative to P27Sc (~25 kT) which is compensated almost equally by the associated gain in electrostatics. However, the surface of P27Sm is more compact, leading to a gain in the non-polar solvation term. Indeed, the WT is characterized by destabilized polar solvation in contrast to the large gains in both mutant states. Such compensations have also been reported in related simulations of the same system that were carried

out using a different force field.[25] In contrast, the W23L mutation causes a major loss in packing leading to severely destabilized van der Waals interactions (~20 *k*T) which is understandable given the nature of the change and the fact that this residue is almost completely buried in the protein; this is associated with less destabilized, compensating electrostatics. This substitution also results in the loss of a crucial H-bond between the NH of the W23 side chain and the backbone carbonyl of L54 (which can lead to a loss of ~4 kcal/mol of relief of strain) and together with local conformational rearrangements, results in unfavourable strain (E_{int} Table S2) which leads to the overall destabilization of this mutant. Although a similar destabilization of internal strains is seen in the helical S mutant, the compensations that accrue as a result of solvation arising from the polar nature of the mutation are much larger, leading to the overall stabilization relative to the WT.

In order to understand why P27Sc is entropically driven we examine the mobility of the two systems. The average fluctuation of P27Sc in complexed state is marginally larger (~20%) than complexed state of P27Sm. We also notice in the principal component (PC) plots (Figure S9) that the space spanned by P27Sc is marginally more widespread, suggestive of larger conformational sampling and hence, higher entropy. We next dissected out the vibrational entropies that are used as the basis of our free energy estimates (Table 1 and Table S2). The total vibrational entropic gain upon the formation of P27Sc is ~7.7 cal/mol/K larger than that of P27Sm. If we examine the entropic contributions along the frequency spectrum[24] we see that the entropic gain in P27Sc originates in the lower frequency part of the spectrum (<150 cm^{-1}) which is understandable as the P27Sc peptide makes more contacts with MDM2 and these are spread out over a larger region of the MDM2 surface than is the case with P27Sm. This leads to a larger effective protein surface which would naturally have a vibrational spectrum that is red-shifted (Figure S10a-c). Indeed, because of a larger number of contacts between the peptide and the protein, the intramolecular interactions of MDM2 have become weaker (Table S2(i) shows a 12% weakening) which makes the protein 'softer' and hence more flexible leading to the observed entropic stabilization.[26]

Movies (M1): MDM2 in surface representation; residues L54, H96, Y100, Y104 are in shown as spheres (only non-hydrogen atoms). The peptides are shown in cartoon (green) with residues F19, W23/L23, L26 and P27/S27 as sticks. The movies are listed below:

File name	Description
M1a_WT.qt	Wild type (WT) complex, (10-15ns) shows that the peptide is stable with an extended C-terminus; Y100 is pointing away from the binding site to accommodate the extended C-terminus of the peptide
M1b_W23L.qt	MDM2-W23L, (10-15ns), peptide conformation is the same as WT; replacement of W with L results in loss of local packing
M1c_P27Sm.qt	MDM2-P27Sm complex (first 1.7ns) shows the flip of Y100 and Y104 towards the binding pocket and stabilizes the peptide in helical conformation. Interaction between Y100 and L54 reduces the size of the binding pocket resulting in a cosier fit. Other key primary interactions are similar to those seen for WT
M1d_P27Sc.qt	MDM2-P27Sc (10-15ns). The C-terminus of the peptide is stabilized in an extended conformation; orientation of the Y100/Y104 is similar to WT.
M1e_P27Sm2.qt	MDM2-P27Sm complex from Trajectory 4 (first 10ns) of Table S1 showing the sampling of Y100.

Reference for this Supporting information:

(1) Kussie, P. H.; Gorina, S.; Marechal, V.; Elenbaas, B.; Moreau, J.; Levine, A. J.; Pavletich, N. P. *Science* **1996**, *274*, 948-953.

(2) MacKerell Jr, A. D.; Bashford, D.; Bellott, M.; Dunbrack Jr., R. L.; Evanseck, J. D.; Field, M. J.; Fischer, S.; Gao, J.; Guo, H.; Ha, S.; Joseph-McCarthy, D.; Kuchnir, L.; Kuczera, K.; Lau, F. T. K.; Mattos, C.; Michnick, S.; Ngo, T.; Nguyen, D. T.; Prodhom, B.; Reiher III, W. E.; Roux, B.; Schlenkrich, M.; Smith, J. C.; Stote, R.; Straub, J.; Watanabe, M.; Wiorkiewicz-Kuczera, J.; Yin, D.; Karplus, M. *J. Phys. Chem. B* **1998**, *102*, 3586-3616.

(3) Darden, T.; York, D.; Pedersen, L. *J. Chem. Phys.* **1993**, *98*, 10089-10092.

(4) Ryckaert, J. P.; Ciccotti, G.; Berendsen, H. J. C. *J. Comput. Phys* 1977, *23*, 327-341.

(5) Im, W.; Feig, M.; Brooks, C. L., 3rd *Biophys. J.* **2003**, *85*, 2900-2918.

(6) Im, W.; Lee, M. S.; Brooks, C. L., 3rd *J. Comput. Chem.* **2003**, *24*, 1691-1702.

(7) Baker, N. A.; Sept, D.; Joseph, S.; Holst, M. J.; McCammon, J. A. *Proc. Natl. Acad. Sci. USA* **2001**, *98*, 10037-10041.

(8) DeLano, W. L.; *The Pymol molecular graphics system, San Carlos, CA USA: DeLano Scientific*: **2002**.

(9) Humphrey, W.; Dalke, A.; Schulten, K. *J. Mol. Graph.* **199**6, *14*, 33-38.

(10) Zondlo, S. C.; Lee, A. E.; Zondlo, N. J. *Biochemistry* **2006**, *45*, 11945-11957.

(11) Chou, P. Y.; Fasman, G. D. *Adv. Enzymol. Relat. Areas Mol. Biol.* **1978**, *47*, 45-148.

(12) Espinoza-Fonseca, L. M.; Trujillo-Ferrara, J. G. *Biopolymers* **2006**, *83*, 365-373.

(13) Uhrinova, S.; Uhrin, D.; Powers, H.; Watt, K.; Zheleva, D.; Fischer, P.; McInnes, C.; Barlow, P. N. *J. Mol. Biol.* **2005**, *350*, 587-598.

(14) Schon, O.; Friedler, A.; Freund, S.; Fersht, A. R. *J. Mol. Biol.* **2004**, *336*, 197-202.

(15) Showalter, S. A.; Bruschweiler-Li, L.; Johnson, E.; Zhang, F.; Bruschweiler, R. *J. Am. Chem. Soc.* **2008**, *130*, 6472-6478.

(16) Vassilev, L. T.; Vu, B. T.; Graves, B.; Carvajal, D.; Podlaski, F.; Filipovic, Z.; Kong, N.; Kammlott, U.; Lukacs, C.; Klein, C.; Fotouhi, N.; Liu, E. A. *Science* **2004**, *303*, 844-848.

(17) Sakurai, K.; Schubert, C.; Kahne, D. *J. Am. Chem. Soc.* **2006**, *128*, 11000-11001.

(18) Grasberger, B. L.; Lu, T.; Schubert, C.; Parks, D. J.; Carver, T. E.; Koblish, H. K.; Cummings, M. D.; LaFrance, L. V.; Milkiewicz, K. L.; Calvo, R. R.; Maguire, D.; Lattanze, J.; Franks, C. F.; Zhao, S.; Ramachandren, K.; Bylebyl, G. R.; Zhang, M.; Manthey, C. L.; Petrella, E. C.; Pantoliano, M. W.; Deckman, I. C.; Spurlino, J. C.; Maroney, A. C.; Tomczuk, B. E.; Molloy, C. J.; Bone, R. F. *J. Med. Chem.* **2005**, *48*, 909-912.

(19) Popowicz, G. M.; Czarna, A.; Rothweiler, U.; Sszwagierczak, A.; Krajewski, M.; Weber, L.; Holak, T. A. *Cell Cycle* **2007**, *6*, 2386-2392.

(20) Fasan, R.; Dias, R. L.; Moehle, K.; Zerbe, O.; Obrecht, D.; Mittl, P. R.; Grutter, M. G.; Robinson, J. A. *Chembiochem* **2006**, *7*, 515-526.

(21) Popowicz, G. M.; Czarna, A.; Holak, T. A. *Cell Cycle* **2008**, *7*, 2441-2443.

(22) Schneider, A.; Dessimoz, C.; Gonnet, G. H. *Bioinformatics* **2007**, *23*, 2180-2182.

(23) McQuarrie, D. A. *Statistical Mechanics*; Harper Row: New York **1976**.

(24) Fischer, S.; Smith, J. C.; Verma, C. S. *J. Phys. Chem. B* **2001**, *105*, 8050-8055.

(25) Lee, H. J.; Srinivasan, D.; Coomber, D.; Lane, D. P.; Verma, C. S. *Cell Cycle* **2007**, *6*, 2604-2611.

(26) Olano, L. R.; Rick, S. W. *J. Am. Chem. Soc.* **2004**, *126*, 7991-8000.